

Motion dynamics of a water drop located on a hydrophobic inclined surface under uniform airflow

Authors

Moshen Bastegani^a
Morteza Bayareh^{a*}

^aDepartment of Mechanical Engineering,
Shahrekord University, Shahrekord, Iran

ABSTRACT

Drop motion on a solid surface has many applications in science and engineering, such as in architecture, offshore structures, and electronics. The present paper aims to simulate the motion of a water droplet located on a hydrophobic inclined surface and investigate its deformation rate using ANSYS FLUENT software. The sessile droplet subjected to uniform airflow can be shed depending on the value of drag and drop's adhesion forces. In the present work, coupled level set and volume of fluid method are employed to estimate the motion of the interface. The effect of drop size, wind velocity, drop contact angle, and drop size on the location, velocity, and drop deformation is investigated. The results demonstrate that the drop is splashed as the contact angle decreases. The drop acceleration has an approximately constant trend at Reynolds numbers ranging from 8000 to 80,000. The maximum acceleration corresponds to the hydrophilic surface and is equal to 0.9 m/s². As the contact angle increases, the acceleration becomes constant. For instance, the drop acceleration is about -0.3 for a contact angle of 135°. The results reveal that the drop requires a longer time to reach the lowest point of the inclined surface by decreasing its diameter and increasing surface hydrophobicity and wind velocity. It is found that as surface hydrophobicity increases, the drop reaches the bottom of the surface in a long time in comparison with the deformed drop.

Article history:

Received : 19 May 2021
Accepted : 13 June 2021

Keywords: Numerical Simulation, Drop, Inclined Surface, Contact Angle, Hydrophobicity, CLSVOF Method.

1. Introduction

The behavior of drops (bubbles) suspended in Newtonian and non-Newtonian fluids is a crucial problem in numerous applications such as hemorheology, fluid mixing, water management in fuel cells, and oil industries [1]. To analyze the dynamics of the interface between two immiscible viscous fluids, the

deformation of the drop (bubble) should be understood. Therefore, the rheology of suspensions and emulsions can be characterized for computational investigations.

The motion mechanism of a suspended drop and the interaction between two drops have attracted interest from many researchers. Bayareh's group [2-5] revealed that the migration time of a drop in a simple shear flow depends on the size of the drop, density and viscosity ratios, Reynolds number, the surface

* Correspond Author: Morteza Bayareh
Department of Mechanical Engineering, Shahrekord University, Shahrekord, Iran
Email: m.bayareh@sku.ac.ir

tension coefficient [2], as well as, initial drop shape [3]. They employed a finite-volume/front-tracking method to solve the governing equations and also evaluated the dynamics of two spherical drops colliding with each other in homogeneous and stratified fluids [4]. It was demonstrated that stratification affects the motion of drops with in-line and side-by-side configurations [5]. In the case of Poiseuille flow, Segre and Silberberg [6] investigated the inertial effect of particle motion for a dilute suspension of solid particles regardless of the buoyancy force for a wide range of Reynolds number and drop size. They found that the solid particles move away from the wall and the axis of the channel, forming a high-concentration layer halfway between the wall and the axis of the channel.

One of the applications of this kind of two-phase flow in engineering sciences is the study of the motion of drops on hydrophobic and hydrophilic solid surfaces. For instance, the presence of liquid droplets on the cathodic surface in proton-exchange fuel cells reduces their performance. Griggs et al. [7] investigated the creeping motion of drops and bubbles under the influence of the gravity force on an inclined surface using the boundary-integral method. They revealed that the drops with lower Bond numbers tend to stay closer to the wall. It was revealed that the deformation of the viscous drop is higher than that of bubbles at a constant Bond number for different inclination angles. Sakai et al. [8] investigated the internal fluidity of a water drop during sliding on an inclined surface experimentally. It was found that the drop velocity is controlled by its rolling and slipping motion. On the hydrophobic surface, the drop with a contact angle of 150° falls with high velocity by slipping, while the drop velocity is controlled by slipping and rolling on a hydrophobic surface with a contact angle of 100° . Dussan [9] considered the effect of external shear force on a small drop located on a planar surface when an immiscible fluid flows parallel to the solid surface. He found that there is a critical strain rate so that the drop does not stick to the surface when the strain rate is lower than the critical one. The wind force required to move the drop adhering to the solid surface was investigated by Durbin [10]. He described the drop deformation and calculated the critical

Weber number based on the critical wind speed to determine the separation distance. It was revealed that the critical Weber number is a function of the contact angle. Kumbur et al. [11], who have done many studies on fuel cells, investigated the effect of controllable engineering parameters, including surface coverage, channel geometry, drop dimensions, and airflow velocity on drop deformation experimentally and analytically. They demonstrated that there is a critical Reynolds number for drop instability in which the drop is removed from the surface. Besides, drop removal is not affected by surface hydrophobicity at low flow rates. Vafaei and Podowski [12] evaluated the correlation between liquid drop size and contact angle and compared their results with experimental data. It was found that the contact angle of axisymmetric drops can be predicted based on their size and material, as well as, surface material. Hashimoto et al. [13] investigated the motion of a water drop on a hydrophobic inclined surface in the presence of wind flow experimentally. They classified the motion of water drop into three stages: sliding, stopping, and climbing. They demonstrated that as the wind velocity increases, the sliding acceleration decreases. When the velocity reaches a certain value, the drop stops and its shape varies from forward-bent to backward-bent. It was reported that drop acceleration is an increasing function of drop deformation in the climbing zone. Mortazavi and Tafreshi [14] studied the behavior of a suspended mixture of drops on an inclined surface and found that drops with less deformation stay farther away from the bottom of the channel. It was revealed that the accumulation of drops in the vicinity of the surface decreases with the inclination angle.

The inclined angle has a significant effect on the drop kinematics during its impact process. Jin et al. [15] experimentally showed that the drop split into smaller ones when the inclined angle is more than 60° . It was also revealed that the gravity force has a larger effect when the inclined angle is enhanced. One of the factors that determine the behavior of drops colliding with a solid surface is hydrophobicity. LeClear et al. [16] introduced a new definition for the Weber number by combining length and velocity scales to

describe the transition from two impact regimes: non-wetting and fully wetted. They showed that the dynamic pressure causes the transition process to begin. Tembely et al. [17] studied the impact process of supercooled drops with superhydrophobic surfaces using the volume of fluid (VOF) method and characterized droplet freezing. It was found that the spreading length increases with the impact velocity and drop the temperature. Xie et al. [18] evaluated the impact of surface wettability on the rolling and sliding of a drop and demonstrated that equilibrium contact angle can be considered as a criterion. They showed that a drop just rolls when the equilibrium contact angle is larger than 147° . Han et al. [19] investigated the oscillation of an adhered oil drop on a solid surface under water due to the amount of drag force and oil-water surface tension. They introduced two regimes of up-down oscillation and left-right oscillations depending on the water flow velocity and drop deformation. Harges et al. [20] investigated the influence of wettability on water drop characteristics under sub-freezing conditions. It was found that the effect of drop size becomes larger for the hydrophilic surface compared to the hydrophobic one.

In the presence of airflow, the detachment of drops on solid surfaces depends on various parameters, including air velocity, wettability, inclination angle, surface tension, etc. [21]. It was found that at Reynolds number of 50 and 100, dynamic pressure and drag force control the drop detachment, respectively [22].

When another drop exists in the vicinity of a sessile drop, the airflow regime is changed, affecting the drag force. In-line [23-24] or side-by-side [25] drops are located on a solid surface. Hooshanginejad and Lee [24] investigated the shedding of a stationary droplet subjected to the wake of a solid hemisphere. It was revealed that when the initial distance between the droplet and the hemisphere is larger than a critical value, the motion of the droplet is independent of the solid hemisphere. Razzaghi and Amirfazli [25] demonstrated that the spacing of droplets determines the critical air velocity for droplets configured side-by-side.

The literature review demonstrates that the issue of drop motion on a solid surface is

limited to experimental investigations [8, 11, 13, 15, 16, 19, 20, 25], theoretical studies [9, 10], or numerical simulations [7, 14, 17]. Numerical simulations used VOF [17], boundary integral [7], and front-tracking [14] methods. To the best of our knowledge, Coupled Level Set and Volume of Fluid (CLSVOF) technique has not been employed to evaluate the dynamics of a sessile drop on an inclined surface in the presence of airflow. Thus, in the present study, the motion of a drop on a hydrophobic inclined surface and its deformation rate is studied using the CLSVOF method. Sec. 2 presents the governing equations. Grid-independence test, validation, and simulation results are given in Sec. 3. The impact of drop size, wind velocity, and contact angle of the drop on the motion of the drop is investigated. Finally, concluding remarks are presented in Sec. 4.

2. Governing equations

The equations that govern the motion of an incompressible drop placed on an inclined surface are continuity and Navier-Stokes equations:

$$\nabla \cdot \vec{u} = 0 \quad (1)$$

$$\rho \frac{\partial \vec{u}}{\partial t} + \rho \nabla \cdot (\vec{u}\vec{u}) = -\nabla p + \nabla \left[\mu (\nabla \vec{u} + \nabla \vec{u}^T) \right] - \int (\sigma k \vec{n}) \delta(\vec{x} - \vec{X}(s,t)) \quad (2)$$

where \vec{u} is the velocity vector, p the pressure, ρ the density, μ the dynamic viscosity, σ the surface tension, and k the curvature for two-dimensional flows. Also, \vec{n} is the unit vector perpendicular to the drop surface and δ is a two-dimensional delta function. \vec{x} and \vec{X} indicate the Eulerian and Lagrangian coordinate systems. The density and viscosity of the drop are indicated by ρ_i and μ_i , respectively. Besides, the density and viscosity of the ambient fluid (airflow) are shown by ρ_o and μ_o , respectively. a is the radius of the undisturbed drop when no force is applied.

The calculation of density and viscosity fields is of particular importance because the physical properties of the flow undergo a discontinuity across the interface between two fluids, leading to numerical diffusion or large fluctuations around the interface. To avoid this

problem, the interface grid is employed which explicitly determines the position of the interface so that the indicator function $I(x)$ is one for the inside of the drop and zero for the outside of the drop. Thus, since ρ and μ inside each fluid are constant, their values at each point of the grid are defined as follows:

$$\begin{cases} \rho(x) = \rho_o + (\rho_i - \rho_o)I(x) \\ \mu(x) = \mu_o + (\mu_i - \mu_o)I(x) \end{cases} \quad (3)$$

The indicator function for the two-dimensional cases is defined as follows:

$$I(x, y) = \frac{1}{2\pi} \int \frac{r \cdot n}{r^2} g(r) ds \quad (4)$$

where ds is the element of the interface. It is more appropriate that the transfer from the inside to the outside of the interface should be done smoothly. For this purpose, the following function is used to define $g(r)$:

$$g(r) = 1 - e^{-\frac{r^2}{\delta^2}} \quad (5)$$

Also, non-dimensional governing parameters are i) Reynolds number $Re = \rho_o UH / \mu_o$, where U is wind velocity and $H = 15h$ is the height of the entrance surface (Fig. 2), ii) Eotvos number $Eo = (\rho_i - \rho_o)(2a)^2 g / \sigma$, iii) density ratio $\lambda = \rho_i / \rho_o$, and iv) viscosity ratio $\eta = \mu_i / \mu_o$.

Normalized time, velocity, and acceleration are $t^* = t\sqrt{g/2a}$, $v^* = v/\sqrt{2ga}$, and $a^* = a/g$, respectively.

3. Results

The motion of a drop of water on a hydrophobic inclined surface is investigated under a uniform wind flow using ANSYS FLUENT software.

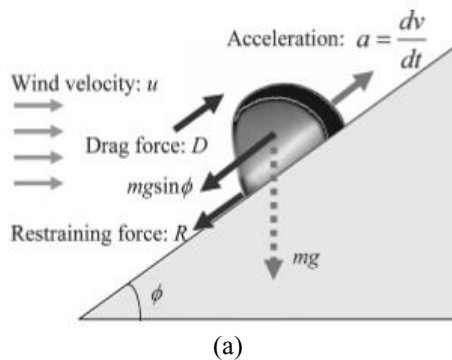


Fig. 1a shows the schematic of the problem and the forces acting on the drop with respect to the direction of droplet motion. The schematic of the present study and boundary conditions are presented in Fig. 2b.

3.1. Grid study

Four grid resolutions of 60271, 86953, 116884, and 177884 are employed to evaluate the effect of grid size on the results. Fig. 2 demonstrates the variations of drop normalized velocity as a function of non-dimensional time for different grid sizes. It is revealed that the values of the dimensionless velocity of drop are the same for the two grid sizes of 116884 and 177884 (the maximum difference is about 4%). Thus, the grid resolution of 116884 is selected for further simulations. It should be pointed out that the grid is more refined in the vicinity of walls and drop surfaces to capture the boundary layer thickness.

3.2. Validation

To verify the present simulations, the work of Hashimoto et al. [13] is used, which experimentally calculated the acceleration of water drops on an inclined solid surface in terms of wind velocity for different drop sizes. Two drops with different masses of 30 mg and 50 mg are selected when the wind velocity is zero and their sliding acceleration is calculated numerically and compared with the results of Hashimoto et al. [13]. Table 1 compares the results obtained from the present simulations and those reported by Hashimoto et al. [13], indicating that there is good agreement between the numerical and experimental results.

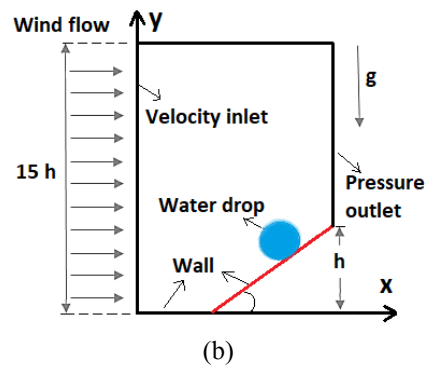


Fig. 1. (a) External forces acting on a drop located on an inclined solid surface [13], (b) schematic of the present problem.

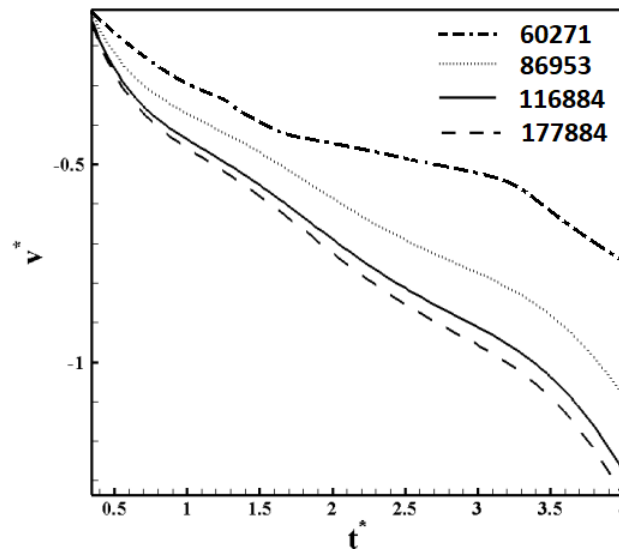


Fig. 2. The normalized velocity of the center of mass of the drop versus dimensionless time for different grid resolutions.

Table 1. Sliding acceleration of a water drop placed on an inclined solid surface.

	m = 30 mg	m = 50 mg
Hashimoto et al. [13]	-0.5	-1.2
Present simulation	-0.59	-1.34

3.3. Effect of wind velocity

Figure 3 illustrates the effect of wind velocity (Reynolds number) on drop deformation for constant values of contact angle, inclination angle, drop size, and fluid properties. It is observed that as the wind velocity increases (the Reynolds number increases); the drop velocity decreases, leading to the drop requiring a longer time to reach the lowest point of the inclined surface. At the Reynolds number of 8837, the drop wets a larger part of the inclined surface due to the lower wind velocity. In other words, the drop spreads more on the surface due to the lower drag force when the Reynolds number is reduced.

As shown in Fig. 4, as the Reynolds number increases the drop travels a shorter distance to reach the lowest point of the surface due to the increase in external forces such as air resistance. The drop slides on the inclined surface over time at Reynolds numbers 8837 and 17674. The dimensionless distance traveled by the drop is greater at a smaller Reynolds number. For example, in dimensionless time of 4, the drop travels the dimensionless distance of about 2.9 and 2.5 at

Reynolds numbers 88369 and 17674, respectively. As the Reynolds number increases, the drop first moves upwards and then moves down in the direction of the inclined surface.

The reason for the initial upward movement is the greater inertial force of the wind compared to the component of the gravitational force and restraining force. After an ascending distance, these forces reach equilibrium and the drop is stopped and then slides down again with a lower acceleration. It is predicted that as the Reynolds number increases further, the duration of the drop ascending increases, and the drop may have a completely ascending motion.

As shown in Fig. 5, as the Reynolds number increases, the drop velocity decreases. The inertial force of the wind resists the gravitational force of the drop. Negative values of velocity indicate downward motion and positive values indicate upward motion of the drop in the direction of the inclined surface. This figure confirms that the drop has an upward motion and then a downward motion at the wind Reynolds number of 88369.

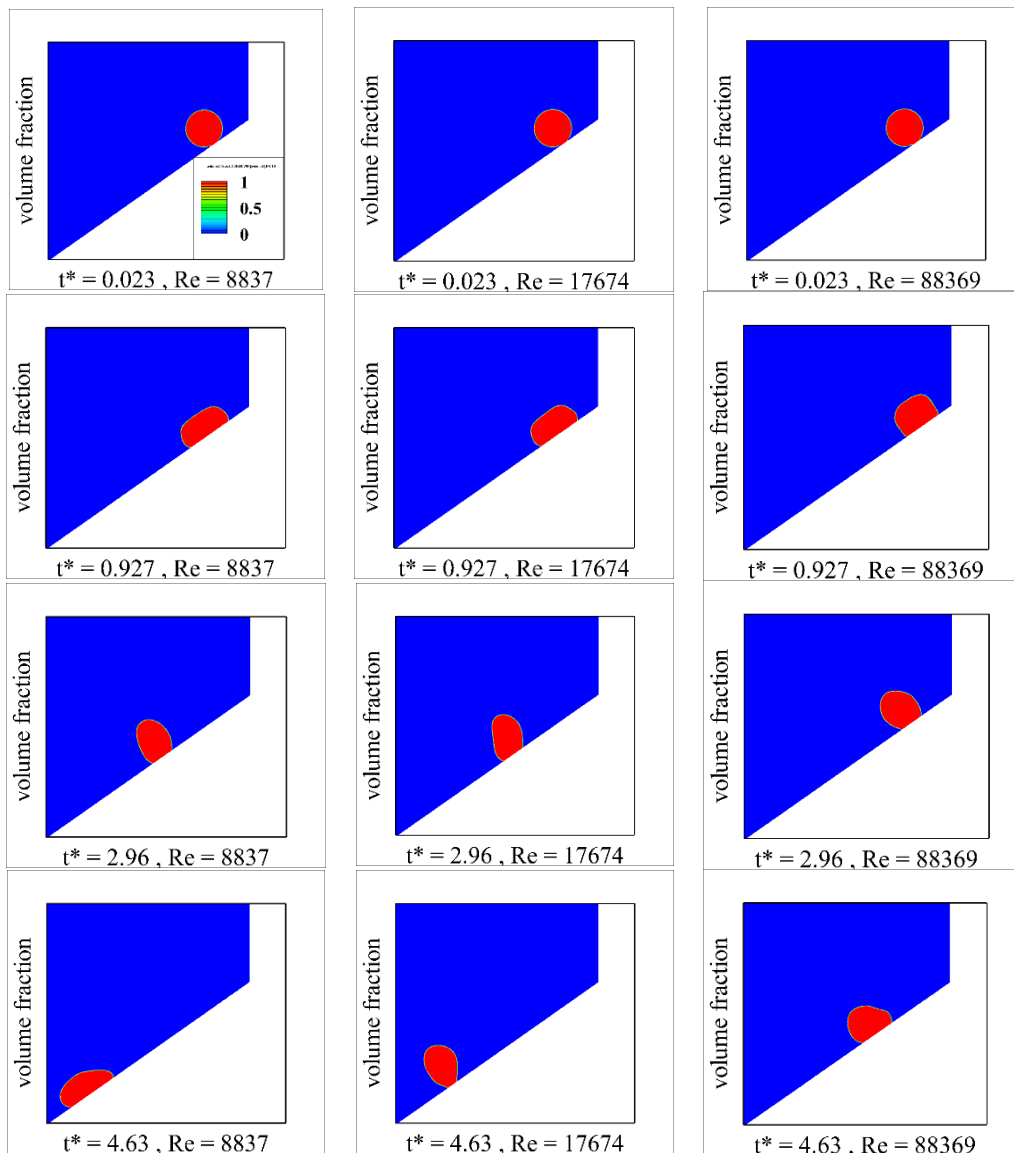


Fig. 3. Time evolution of the sliding motion of drops on a solid surface for $Eo = 3, \lambda = 815, \eta = 56, \varphi = 35^\circ, \beta = 135^\circ$, and different Reynolds numbers.

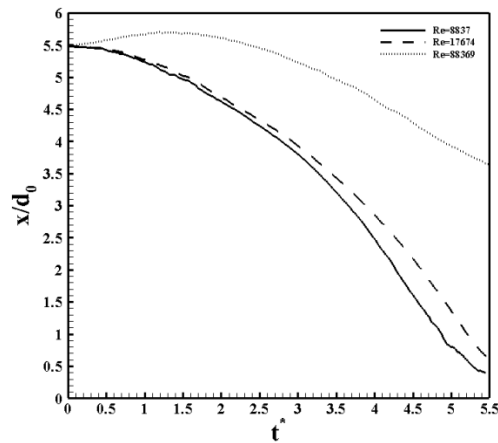


Fig. 4. Normalized position of the center of mass of the drop in terms of dimensionless time for $Eo = 3, \lambda = 815, \eta = 56, \varphi = 35^\circ, \beta = 135^\circ$, and different Reynolds numbers.

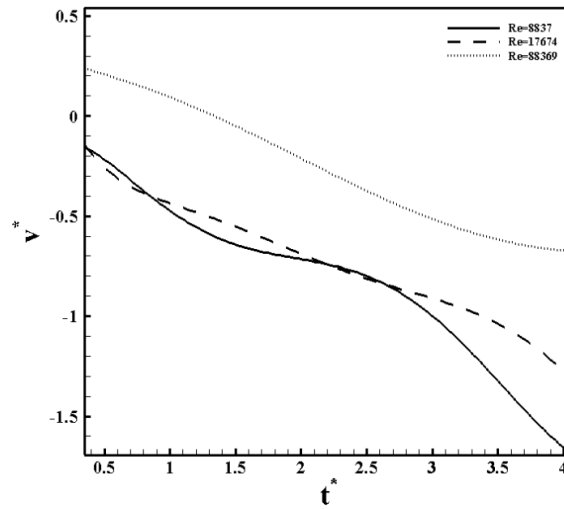


Fig. 5. Normalized velocity of the center of mas of the drop in terms of dimensionless time for $Eo = 3, \lambda = 815, \eta = 56, \varphi = 35^\circ, \beta = 135^\circ$, and different Reynolds numbers.

Figure 6 shows that the drop acceleration has an approximately constant trend at Reynolds numbers ranging from 8000 to 80,000. At the Reynolds number 8837, the dimensionless acceleration of the droplet is not uniform and oscillates with an amplitude of about 0.7. However, the drop moves down all the time. The motion of the drop is almost regular and sometimes its acceleration is zero. As the wind inertia increases and the Reynolds number reaches 17676, the drop accelerates almost

uniformly, except at the beginning and the end. At Reynolds number 88369, the acceleration of the drop is almost constant, showing the balance between the forces exerted on the drop by increasing the Reynolds number. It is predicted that at a certain Reynolds number, the drop will be completely stopped and then move upwards as the Reynolds number increases. The acceleration of the upward movement will be first constant and then oscillating with a large range of variations.

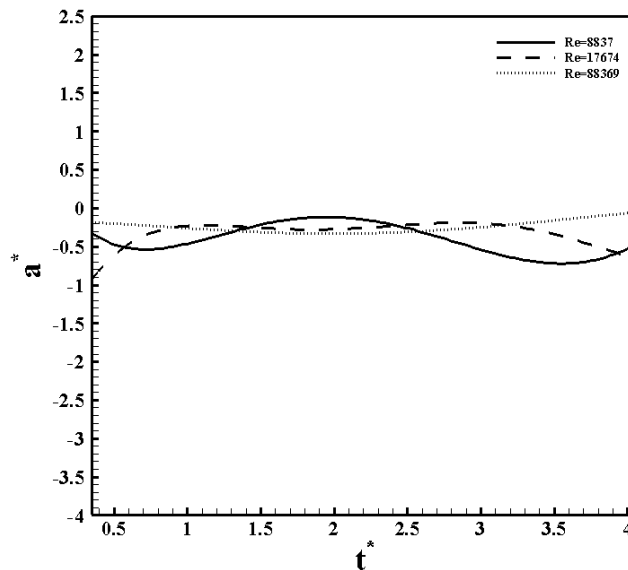


Fig. 6. Normalized acceleration of the center of mass of the drop in terms of dimensionless time for $Eo = 3, \lambda = 815, \eta = 56, \varphi = 35^\circ, \beta = 135^\circ$, and different Reynolds numbers.

3.4. Effect of contact angle (β)

Figure 7 shows the effect of contact angle on drop deformation at different times. As shown in this figure, as the contact angle increases, i.e., surface hydrophobicity increases, the drop deformation is reduced and its spherical shape is retained. In this case, the center of the drop reaches the bottom of the surface in a long time in comparison with the deformed drop. If the contact angle is less than 90° , the surface is hydrophilic and the drop tends to

spread on the surface. For this reason, the effective surface area in calculating the drag force decreases, the shape coefficient decreases, and the drop fluid (not the drop center of mass) reaches the lower edge of the inclined surface faster. It can be concluded that at contact angles less than 90° , the probability of drop separation increases. If the contact angle is greater than 90° , the surface is hydrophobic and the tendency to drop to spread on the surface increases.

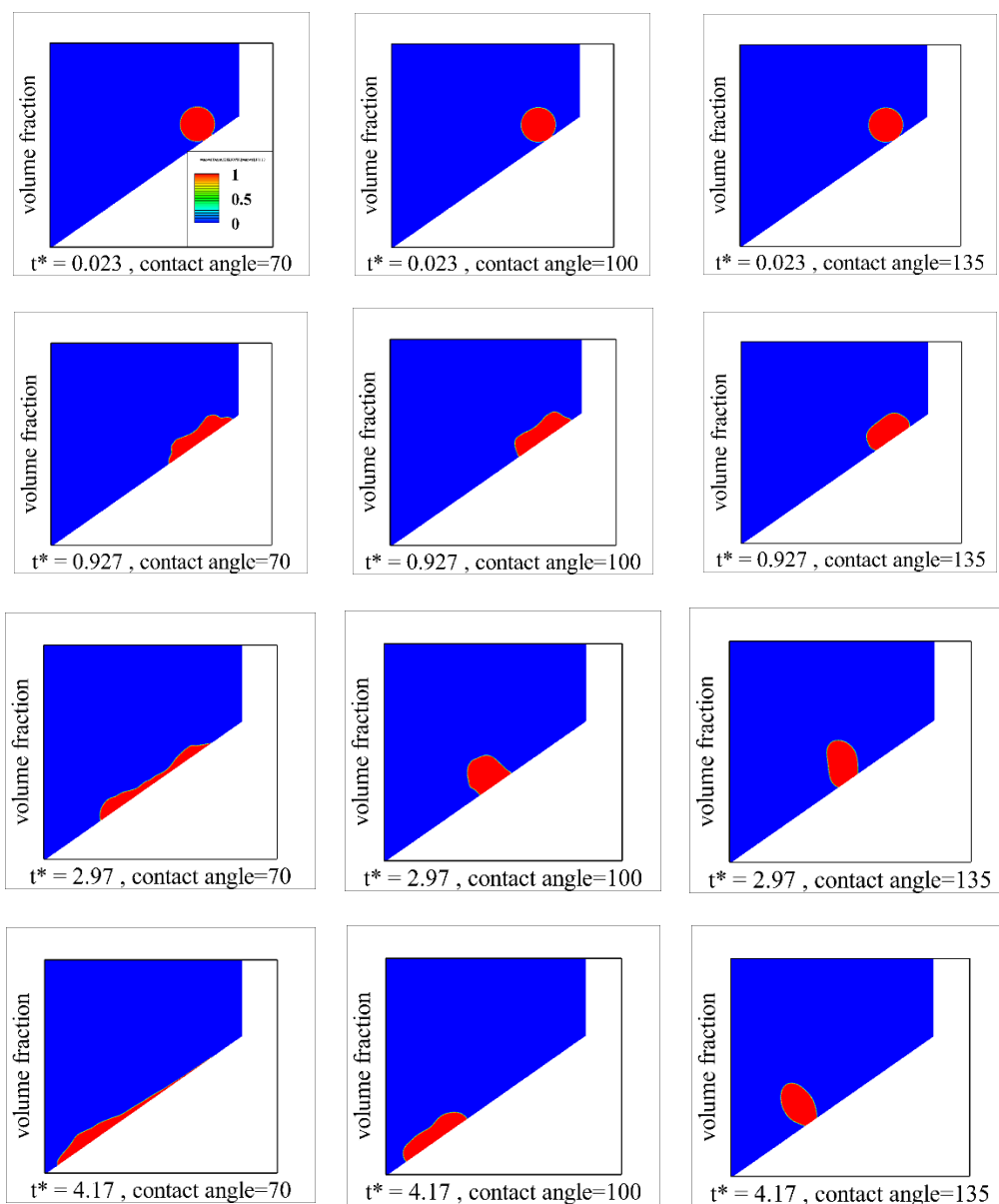


Fig. 7. Time evolution of the sliding motion of drops on a solid surface for $Eo = 3$, $\lambda = 815$, $\eta = 56$, $\varphi = 35^\circ$, $Re = 17674$, and different contact angles.

As shown in Fig. 8, the time in which the drop reaches the lower edge of the inclined surface is shorter for smaller contact angles due to greater wetting surface area. As can be seen, at the contact angle of 70° , a jump occurred at about $t^* = 2.7$. This is due to the drop spreading when it is close to the separation mode. Hence, parts of the top and bottom of the drop are connected by a thin surface and move in different directions, meaning that the shear surface forms in the middle region of the drop and causes the drop to completely break up over time and wet the solid surface.

For a contact angle of 70° , the drop initially moves faster (the slope of the velocity curve is higher) compared to the contact angles of 100° and 135° (Fig. 9). This is due to that the drop spreads faster. The splashed drop loses its spherical shape and less drag is applied to it. It is

also observed that velocity fluctuations are greater at smaller contact angles. When the droplet is almost splashed at a contact angle of 70° , its velocity decreases at about $t^* = 2.7$. At this time, the part of the fluid, which is above the mass center of the drop, is splashed in the front region of the mass center. When almost all of the drop fluid is placed on the surface at about $t^* = 3.6$, the drop swells on the surface. This decrease and increase in velocity are affected by the contact angle. The variation of velocity is smaller for larger contact angles. Therefore, at larger contact angles, the drop has an almost constant acceleration. The maximum acceleration corresponds to the hydrophilic surface and is equal to 0.9 m/s^2 . As the contact angle increases, this amplitude of velocity fluctuations decreases, and the acceleration becomes constant. For instance, the drop acceleration is about -0.3 for a contact angle of 135° .

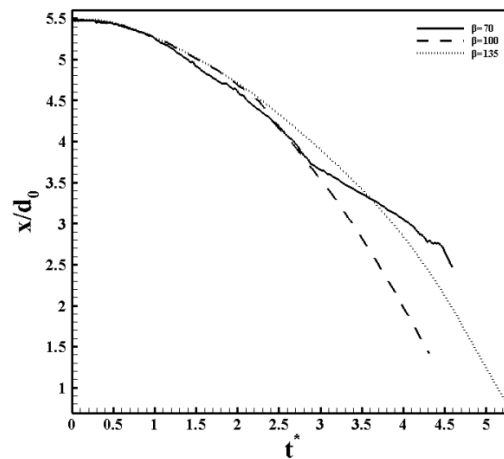


Fig. 8. Normalized position of the center of mass of the drop in terms of dimensionless time for $Eo = 3$, $\lambda = 815$, $\eta = 56$, $\varphi = 35^\circ$, $Re = 17674$, and different contact angles.

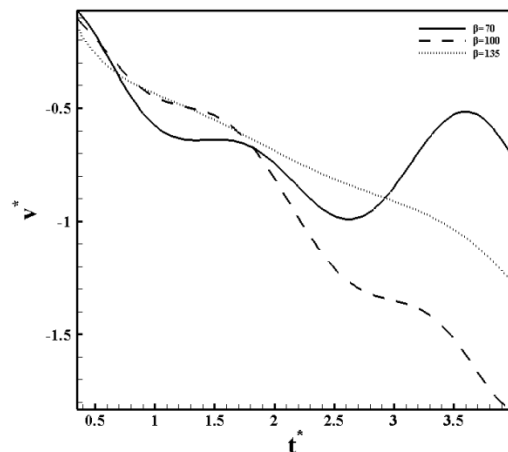


Fig. 9. Normalized velocity of the center of mass of the drop in terms of dimensionless time for $Eo = 3$, $\lambda = 815$, $\eta = 56$, $\varphi = 35^\circ$, $Re = 17674$, and different contact angles.

3.5. Effect of drop size

Figure 10 demonstrates that the larger drops travel a longer distance at the same time. Larger drops have more acceleration due to higher inertia at the same dimensionless times. Also, because the cross-sectional area of the drop affected by the drag force is larger, the drop undergoes more deformation. The deformation force also helps the larger drop to reach the lower edge of the inclined surface faster. Conversely, smaller drops have a smaller gravity force component

along the inclined surface, resulting in lower velocity. Also, smaller drops exhibit less deformation.

Figure 11 shows that the beginning motion of drops is not the same for drops with different diameters due to various locations of the center of drops. However, larger drops travel the entire distance of the inclined surface faster due to the dominance of gravity over drag and friction forces. The smaller drop travels the same path at a larger dimensionless time due to the larger effect of wind flow.

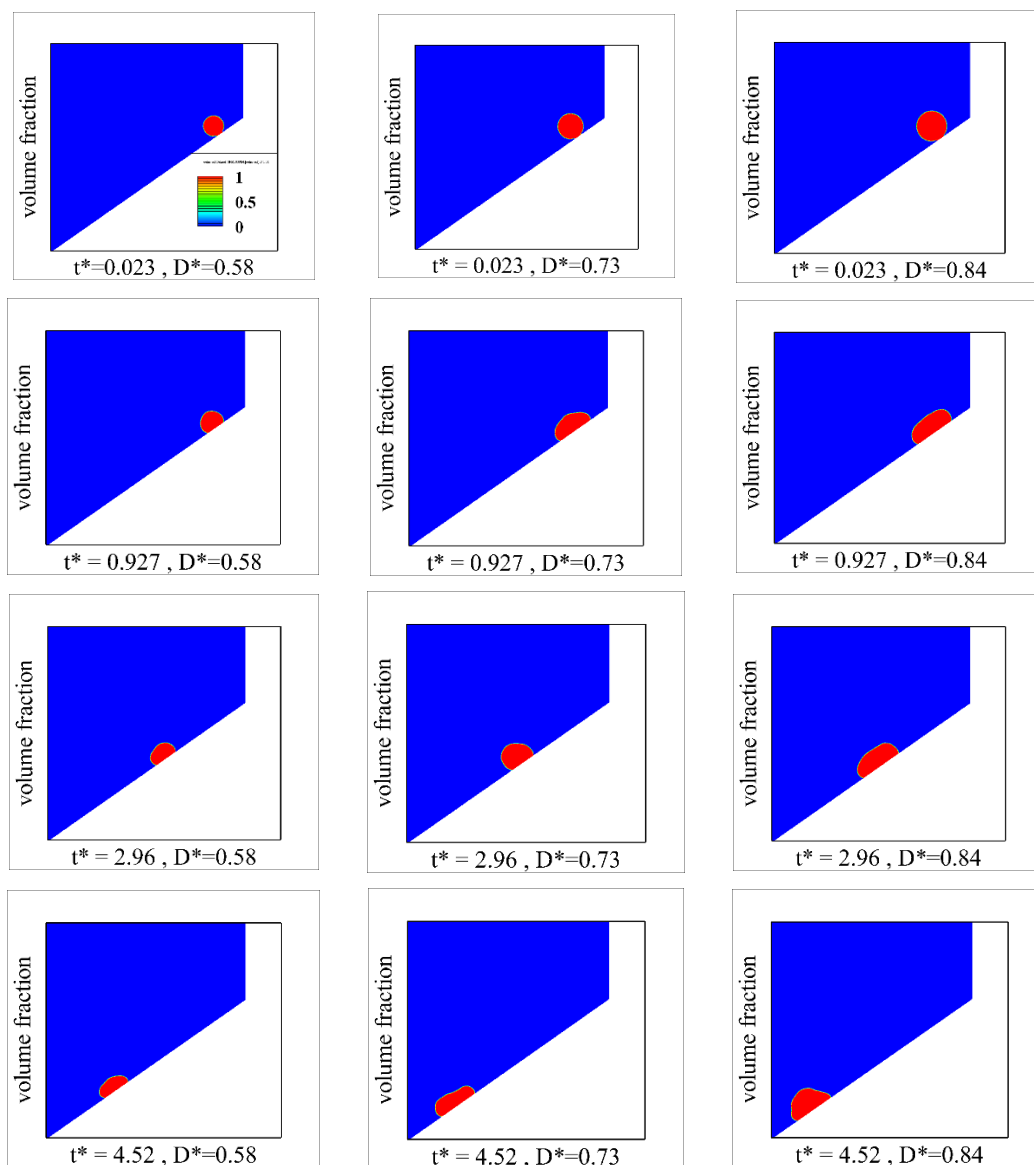


Fig. 10. Time evolution of the sliding motion of drops on a solid surface for $Eo = 3$, $\lambda = 815$, $\eta = 56$, $\varphi = 35^\circ$, $Re = 17674$, and different drop diameters.

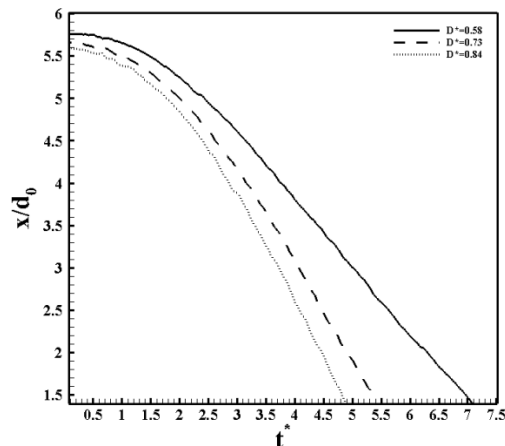


Fig. 11. Normalized position of the center of mass of the drop in terms of dimensionless time for $Eo = 3$, $\lambda = 815$, $\eta = 56$, $\phi = 35^\circ$, $Re = 17674$, and different drop diameters.

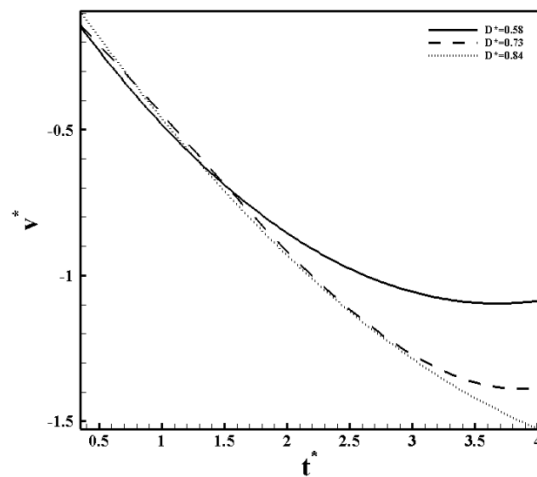


Fig. 12. Normalized velocity of the center of mass of the drop in terms of dimensionless time for $Eo = 3$, $\lambda = 815$, $\eta = 56$, $\phi = 35^\circ$, $Re = 17674$, and different drop diameters.

As shown in Fig. 12, the larger drops have a higher velocity at their beginning motion at the same dimensionless times. Their velocity decreases as the drop moves downward and the effect of wind flow increases. At some times the velocity of the smaller drops is greater than the velocity of the larger ones due to the increase in the cross-sectional area of the larger drop and larger drag force. This figure reveals that the acceleration decreases with increasing time. As the size of the drop is enhanced, its acceleration decreases.

4. Conclusions

Drop motion on a solid surface has a variety of applications, such as wind turbines, offshore structures, and electronics. In this study, the

motion dynamics of a drop placed on a hydrophobic inclined surface and its deformation rate were investigated using ANSYS FLUENT software. The main objective of the present work was the use of a CLSVOF method to estimate the motion of the interface. The results demonstrated that as the wind velocity increases (the Reynolds number increases); the drop velocity decreases, leading to the drop requiring a longer time to reach the lowest point of the inclined surface. For example, in dimensionless time of 4, the drop travels the dimensionless distance of about 2.9 and 2.5 at Reynolds numbers 88369 and 17674, respectively. It was found that as surface hydrophobicity increases, the drop reaches the bottom of the surface in a long time in comparison with the deformed drop. The results

revealed that larger drops require a shorter time to reach the lowest point of the inclined surface. The maximum acceleration corresponds to the hydrophilic surface and is equal to 0.9 m/s^2 . As the contact angle increases, this amplitude of velocity fluctuations decreases, and the acceleration becomes constant. For instance, the drop acceleration is about -0.3 for a contact angle of 135° .

Conflict of interest: The authors declare that they have no conflict of interest.

References

- [1] Bayareh M, Mortazavi S (2011) Effect of density ratio on the hydrodynamic interaction between two drops in simple shear flow, *Iranian Journal of Science and Technology*, 35: 121-132
- [2] Bayareh M, Mortazavi S (2009) Numerical simulation of the motion of a single drop in a shear flow at finite Reynolds numbers, *Iranian Journal of Science and Technology*, 33: 441-452.
- [3] Mohammadi Masiri S, Bayareh M, Ahmadi Nadooshan A (2019) Pairwise interaction of drops in shear-thinning inelastic fluids, *Korea-Australia Rheology Journal* 31(1): 25-34.
- [4] Armandoost P, Bayareh M, Ahmadi Nadooshan A (2018) Study of the motion of a spheroidal drop in a linear shear flow. *Journal of Mechanical Science and Technology*. 32: 2059-2067.
- [5] Bayareh M, Dabiri S, Ardekani AM (2016) Interaction between two drops ascending in a linearly stratified fluid, *European Journal of Mechanics-B/Fluids*, 60: 127-136. <http://dx.doi.org/10.1016/j.euromechflu.2016.07.002>
- [6] Segre G, Silberberg A (1962) Behaviour of macroscopic rigid spheres in Poiseuille flow Part I. Determination of local concentration by statistical analysis of particle passages through crossed light beams. *Journal of Fluid Mechanics*. 14: 115-135.
- [7] Griggs A J, Zinchenko AZ, Davis R. H (2008) Gravity-driven motion of a deformable drop or bubble near an inclined plane at low Reynolds number. *International Journal of Multiphase Flow*. 34: 408-418.
- [8] Sakai M, Song JH, Yoshida N, Suzuki S, Kameshima Y, Nakajima A (2006) Direct observation of internal fluidity in a water droplet during sliding on hydrophobic surfaces. *Langmuir*. 22: 4906-4909.
- [9] Dussan EB, (1988) On the ability of drops to stick to surfaces of solids. 3. The influences of the motion of the surrounding fluid on dislodging drops. *J. Fluid Mech*. 174: 381-397.
- [10] Durbin A (1988) On the wind force needed to dislodge a drop adhered to a surface. *Journal of Fluid Mechanics*. 196: 205-222.
- [11] Kumbur EC, Sharp KV, Mench MM (2006) Liquid droplet behavior and instability in a polymer electrolyte fuel cell flow channel. *Journal of Power Sources*. 161: 333-345.
- [12] Vafaei S, Podowski MZ (2005) Analysis of the relationship between liquid droplet size and contact angle. *Advances in Colloid and Interface Science*. 113: 133-146.
- [13] Hashimoto A, Sakai M, Song H, Yoshida N, Suzuki S, Kameshima Y, Nakajima A (2008) Direct observation of water droplet motion on a hydrophobic self-assembled monolayer surface under airflow. *Journal of The Surface Finishing Society of Japan*. 59: 907-919.
- [14] Mortazavi S, Tafreshi MM (2013) On the behavior of suspension of drops on an inclined surface. *Physica A: Statistical Mechanics and its Applications*. 392: 58-71.
- [15] Jin Z, Zhang H, Yang Z (2016) The impact and freezing processes of a water droplet on a cold surface with different inclined angles. *International Journal of Heat and Mass Transfer*, 103: 886–893. doi:10.1016/j.ijheatmasstransfer.2016.08.012
- [16] LeClear S, LeClear J, Abhijeet Park K-C, Choi W (2016) Drop impact on inclined superhydrophobic surfaces. *Journal of Colloid and Interface Science*, 461: 114–121. doi:10.1016/j.jcis.2015.09.026
- [17] Tembely M, Attarzadeh R, Dolatabadi A (2018) On the numerical modeling of supercooled micro-droplet impact and freezing on superhydrophobic surfaces. *International Journal of Heat and Mass*

- Transfer, 127: 193–202.
doi:10.1016/j.ijheatmasstransfer.2018.06.104
- [18] Xie J, Xu J, Shang W, Zhang K (2018) Mode selection between sliding and rolling for droplet on inclined surface: Effect of surface wettability. *International Journal of Heat and Mass Transfer*, 122: 45–58.
doi:10.1016/j.ijheatmasstransfer.2018.01.098
- [19] Han Y, He L, Wang S, Luo X, Zhou R (2020) Oscillation behaviors of oil droplets adhered on the solid surfaces with different wettability in a laminar flow field. *Experimental Thermal and Fluid Science*, 110057.
doi:10.1016/j.expthermflusci.2020.110057
- [20] Harges E, Cremaschi L, Adanur B (2021) Distribution, coalescence, and freezing characteristics of water droplets on surfaces with different wettabilities under subfreezing convective flow, *Applied Thermal Engineering*, 182: 116052.
<https://doi.org/10.1016/j.applthermaleng.2020.116052>
- [21] Roisman I V, Criscione A, Tropea C, Mandal D K, Amirfazli A (2015) Dislodging a sessile drop by a high-Reynolds-number shear flow at subfreezing temperatures. *Physical Review E*, 92(2).
doi:10.1103/physreve.92.023007
- [22] Carroll B, Hidrovo C (2013) Droplet Detachment Mechanism in a High-Speed Gaseous Microflow. *Journal of Fluids Engineering*, 135(7): 071206.
doi:10.1115/1.4024057
- [23] Moghtadernejad S, Jadidi M, Esmail N, Dolatabadi A (2016) Shear-driven droplet coalescence and rivulet formation. *Proc. Inst. Mech. Eng. C: J. Mech. Eng. Sci.*, 230: 793-803.
- [24] Hooshanginejad A, Lee S (2017) Droplet depinning in a wake. *Phys. Rev. Fluids.*, 2: 031601.
- [25] Razzaghi A, Amirfazli A (2018) Shedding of a Pair of Sessile Droplets. *International Journal of Multiphase Flow*.
doi:10.1016/j.ijmultiphaseflow.2018.08.011